Human-robot formation control via visual and vibrotactile haptic feedback

Stefano Scheggi, *Member, IEEE,* Fabio Morbidi, *Member, IEEE,*
and Domenico Prattichizzo, *Member, IEEE*

Abstract—In this paper we present a new visuo-haptic interaction mechanism for human-robot formation control. The formation setup consists of a human leader and multiple follower robots. The mobile robots are equipped only with RGB-D cameras, and they should maintain a desired distance and orientation to the leader at all times. Mechanical limitations common to all the robots limit the possible trajectories that the human can take. In this regard, vibrotactile feedback provided by a haptic bracelet guides the human along trajectories that are feasible for the team by warning her/him when the formation constraints are being violated. Psychophysical tests on the bracelet together with real-world experiments conducted with a team of Pioneer robots show the effectiveness of the proposed visuo-haptic paradigm for the coordination of mixed human-robot teams.

Index Terms—Haptic I/O, Design for wearability, Human-robot team, Vibrotactile feedback, Autonomous vehicles

1 Introduction

MOBILE robots hold a great promise in assisting people in a large variety of domains, including medical, military, recreational, and industrial applications [1], [2]. Robots, indeed, can support humans in complex everyday tasks, such as indoor and outdoor navigation, information supply and carrying of heavy objects. However, a mobile robot capable of reliably interacting with humans needs several advanced skills such as detection of the targeted subject, recognition of the environment surrounding it, and collision avoidance.

This paper considers a *mixed human-robot team* where a human leader is followed by a group of N unicycle robots (see Fig. 1). Recent studies [3], [4] have shown a close relationship between the shape of human locomotor paths in goal-directed movements, and the simplified kinematic model of a wheeled mobile robot. Thus, nonholonomic constraints similar to those of mobile robots seem to be at work when a human is walking: in particular, it has been shown in [3], [4] that the shoulders can be considered as a sort of steering wheel that drives the human body with a short delay (of about one fifth of a second). These results provided us with the theoretical ground for adapting the leader single-follower formation control strategy proposed in [5] for unicycles, to a mixed human-robot team. The team moves in an unstructured environment, and the robots do not need any a priori metric information about it. The goal of the robot followers is to maintain a certain desired distance and orientation with respect to the human leader at all times. Note that the *non-rigid* nature of the formations considered in [5] provides us with flexibility and robustness against noisy measurements.

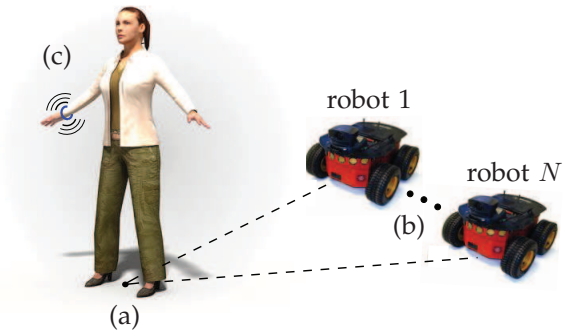

Fig. 1. The proposed setup consists of a human leader (a), and a team of N mobile robots (b), solely equipped with RGB-D cameras. The robots estimate the human motion through the RGB-D sensors and use such information to follow the leader according to the formation parameters. A vibrotactile bracelet (c), warns the leader about potential violations of the formation constraints.

In the formation control strategy proposed in [5], the forward velocity of the robot leader and the curvature of its trajectory should respect suitable constraints at all times. To achieve this goal in the mixed setup of this paper, our idea is to introduce a second communication channel between the follower robots and the human leader. In fact, the followers do not estimate only the human motion using the on-board RGB-D cameras, but they also send easily-processable information to the leader, e.g., to warn her/him that she/he is walking too fast and that the robots cannot

- *S. Scheggi and D. Prattichizzo are with the Department of Information Engineering and Mathematics, University of Siena, 53100 Siena, Italy. D. Prattichizzo is also with the Department of Advanced Robotics, Istituto Italiano di Tecnologia, 16163 Genova, Italy. E-mail: {scheggi, prattichizzo}@dii.unisi.it*
- *F. Morbidi is with the NeCS team, INRIA Grenoble Rhône-Alpes, 38334 Montbonnot Saint-Martin, France. E-mail: fabio.morbidi@inria.fr*

keep up. In this way, the cohesiveness and reactivity of the team can be significantly improved.

Noninvasive human-robot interaction can be easily achieved via a *wearable haptic device* that provides vibrotactile feedback to the user. In fact, visual and auditory channels may be overloaded with information, thus resulting in a rapid error increase and in a consequent reduction in overall user performance. A possible solution to this problem is to deliver this information through an underutilized sensory channel. As with sound, a tactile stimulus is made up of a signal with varying frequency and amplitude, but differently from the auditory feedback which needs a mental model in order to parse the information, tactile feedback directly engages our motor learning system [6]. While kinesthetic feedback is common in haptic systems, vibrotactile feedback is used in this work because tactile devices are generally more portable and less encumbering than kinesthetic devices and have a wider range of action [7].

In this paper an intuitive *haptic bracelet* is designed to correct the trajectory of the human leader, according to the formation specifics. The proposed setup presents significant advantages: (*i*) the robots are minimally equipped: they have only an off-the-shelf RGB-D camera onboard, e.g., Microsoft's Kinect, from which they obtain all the information necessary to implement their control law (however, other sensors, such as time-of-flight (ToF) cameras, could be used as well for the same purpose); (*ii*) differently from [5] no global information is needed, i.e., each follower requires only the pose of the human leader with respect to its local reference frame; (*iii*) the setup is modular and scalable: in fact, since each robot is uniquely engaged with the leader, new followers can be easily added or removed from the team.

This work is based in part on previous conference material [8] compared to which we provide herein a new and improved prototype of the haptic bracelet, a robust visual human-tracking algorithm, a more extended theory and a more comprehensive experimental validation.

1.1 Related work and organization

Several recent works have studied *human-robot interaction* in leader-follower systems: however, none of them considered human multi-robot cooperation via haptic feedback.

In [9] the authors proposed a laser-based person-tracking method and investigated the social perception of a robot's movement as it follows the human. The authors designed two person-following modes and analyzed which one is more natural and socially acceptable. The tracking method is based on a single laser range finder and a simple proportional feedback control is employed based on the error between the robot's current distance to the person and the desired distance. The robot notifies the person if she/he is walking too fast by using synthesized computer speech. Closely related is the work in [10] where the authors presented a robotic system capable of person following and responding to verbal and non-verbal commands in the presence of varying lighting conditions and uneven floor. In particular, they used a real-time depth map obtained from a CSEM SwissRanger ToF camera which can properly work both in total darkness and in bright light, and leveraged a PID controller and a Kalman filter for the person following and estimation tasks, respectively. The user communicates with the robot using a set of predefined gestures and a verbal vocabulary while the robot verbally reports its status to her/him. In [11], the authors dealt with human-machine interaction in a structured environment using multiple intelligent sensors. The sensor network recognizes the human target and the mobile robot, and provides control commands to it. A virtual spring model is used for describing the interaction between the human and the mobile robot, which guarantees smooth control inputs and good target-tracking performance. Although multiple robots can be potentially used, the authors focused on a single robot interacting with a human. Moreover the assumption of a structured environment plays a crucial role in this approach. Recently, experiments on the coordination of human-robot teams have been carried out in [12]: this represents one of the first attempts of human guidance via decentralized control of a team of robots. However, differently from our work the authors mainly focused on the formation control design, and they did not exploit the non-holonomic nature of human locomotion. Finally, it is worth mentioning [13] where the authors studied human-robot teams for exploring an unmapped indoor area. The human carries an IMU sensor which is devoted to localization and tracking in conjunction with laser range finders mounted on the robots and a laptop which is used to display visual information to her/him. When compared with our approach based on a simple vibrotactile bracelet, this solution is seemingly bulkier and less practical.

Regarding the haptic feedback, most of the existing research on *cutaneous stimulation* has focused on providing stimuli on human finger pads, due to the high number of receptors located there. Recent works, however, have started to explore other body parts for information display. In particular, vibrotactile devices have been mainly used to adjust the posture of specific portions of the body. For example, in [6] the authors developed a robotic suit for improved human motor learning, which provides vibrotactile feedback proportional to the error between the effective and the learned motion. Closely related is the work in [14], which presents a wearable robotic teacher for guiding forearm movements. The system provides vibrotactile stimuli through a bracelet composed of four vibration motors disposed in quadrants. Along the same line, in [15], a physiological study was conducted to verify the effectiveness of different wrist-worn

tactor placements for delivering spontaneous alerts and notifications to human subjects. A vibrotactile orientation guidance device was proposed in [16]. The authors mainly focused here on the layout of the device as well as on the generation of different vibration patterns. Finally in [17], an evaluation of five tactile devices for wrist rotation guidance was presented. Closer to our research are [18], [19] where the authors studied the possibility of presenting guidance information on a vibrotactile waist belt integrated with a directional sensor and a GPS system. Results indicated the usefulness of tactile feedback for navigation purposes as well as for situational awareness in multi-task environments. However, [18], [19] do not consider the vibrotactile feedback as a possible communication channel for human-robot interaction.

Differently from the papers mentioned above, in this work we consider a *mixed* formation where multiple follower robots track a human leader using *only* their on-board RGB-D cameras. The nonlinear control strategy proposed in [5] has been adapted to the particular setup considered in this paper, and an additional communication channel has been introduced between the human leader and the followers: simple vibrotactile signals delivered by a custom-designed haptic bracelet are used to warn the leader about potential violations of the formation constraints.

The rest of the paper is organized as follows. Sect. 2 reviews the formation control strategy presented in [5] and introduces a simple collision-avoidance policy for the followers. Sect. 3 presents our method for detecting and tracking a human subject using an RGB-D camera. Sect. 4 describes the main features of our haptic bracelet. In Sect. 5 we validate the proposed algorithms via extensive numerical tests and real-world experiments. Finally, in Sect. 6 we summarize the main contributions of the paper, and discuss possible avenues for future research.

2 Leader-follower formation control strategy

In this section we briefly review the leader-follower formation control strategy proposed in [5] that we adapt to our mixed human-robot setup. In particular, instead of considering the robot's pose expressed in a global reference frame as in [5], the position and orientation of the leader will be here estimated in the followers' reference frames.

We assume that a robot $\mathbf{R} = (x,\, y,\, \theta)^T$ with initial pose $\overline{\mathbf{R}} \in \mathbb{R}^2 \times \mathcal{S}^1$ and control $(v,\, \omega)^T \in \mathbb{R}_{>0} \times \mathbb{R}$ satisfies,

$$\begin{cases} \dot{x} = v\cos\theta,\ \dot{y} = v\sin\theta,\ \dot{\theta} = \omega, \\ (x(0),\ y(0),\ \theta(0))^T = \overline{\mathbf{R}}. \end{cases}$$

We set $\kappa(t) = \omega(t)/v(t)$ which is the curvature of the path followed by the robot at time t. Denote by $\mathbf{P}(t) = (x(t),\, y(t))^T$ the position of $\mathbf{R}$ at time t, $\theta(t)$ its heading, $\boldsymbol{\tau}(\theta) = (\cos\theta,\, \sin\theta)^T$ the normalized velocity vector and $\boldsymbol{\nu}(\theta) = (-\sin\theta,\, \cos\theta)^T$ the normalized vector orthogonal to $\boldsymbol{\tau}(\theta)$. $\mathbf{R}$ is said to satisfy the *trajectory constraint* $(V,\, K^-,\, K^+)$ if $\forall\, t \geq 0$,

$$0 \,<\, v(t) \,\leq\, V, \tag{1}$$

$$K^- \,\leq\, \kappa(t) \,\leq\, K^+. \tag{2}$$

Let V_p, K_p^- and K_p^+ be three constants. In the remainder of this paper, we will suppose that every robot satisfies the physical constraint $(V_p,\, K_p^-,\, K_p^+)$, which represents the mechanical limitation common to all the vehicles.

Let us now turn our attention to the *formation specification*, and suppose that $\mathbf{R}_0 = (\mathbf{P}_0^T,\, \theta_0)^T$ is the formation *leader* and $\mathbf{R}_i$, $i \in \{1, \ldots, N\}$, the *followers*. Let $d_i > 0$, $\phi_i : |\phi_i| < \pi/2$ be the assigned parameters that define the formation shape (see Fig. 2). We then say that $\mathbf{R}_0$ and $\mathbf{R}_i$ are in (d_i, ϕ_i)-formation with leader $\mathbf{R}_0$ at time t, if the error

$$\mathbf{E}_i(t) \,\triangleq\, \mathbf{P}_0(t) - d_i\, \boldsymbol{\tau}(\phi_i) \,=\, \mathbf{0}, \tag{3}$$

and, simply, that $\mathbf{R}_0$ and $\mathbf{R}_i$ are in (d_i, ϕ_i)-formation with leader $\mathbf{R}_0$, if (3) holds for all $t \geq 0$. Moreover, we say that $\mathbf{R}_0$ and $\mathbf{R}_i$ are asymptotically in (d_i, ϕ_i)-formation with leader $\mathbf{R}_0$ if $\lim_{t\to\infty} \mathbf{E}_i(t) = \mathbf{0}$. Obviously, if the team consists of N followers, N pairs of distance and orientation constraints (d_1, ϕ_1), …, (d_N, ϕ_N) need to be simultaneously enforced between the leader and the robots. Set $d_i > 0$, $\phi_i : |\phi_i| < \pi/2$ and suppose that $\mathbf{R}_0$ satisfies the trajectory constraint (V_0, K_0^-, K_0^+). If the following conditions hold:

$$\begin{gathered} -\tfrac{1}{d_i} < K_0^- \leq K_0^+ < \tfrac{1}{d_i \cos\phi_i},\ \text{ if }\ \phi \geq 0, \\ -\tfrac{1}{d_i \cos\phi_i} < K_0^- \leq K_0^+ < \tfrac{1}{d_i},\ \text{ if }\ \phi < 0, \\ \widetilde{K}_0^- < K_0^- \leq K_0^+ < \widetilde{K}_0^+, \end{gathered} \tag{4}$$

$$\begin{aligned} V_0 \cos\big(\min(0, (\arcsin(K_0^+ d_i \cos\phi_i) - \phi_i)\,, \\ (\phi_i - \arcsin(K_0^- d_i \cos\phi_i)))\big) < V_p\, \cos\phi_i, \end{aligned} \tag{5}$$

where $\widetilde{K}_0^{\pm} = (\text{sign}\ K_p^{\pm})\big(((K_p^{\pm})^{-1} - d_i \sin\phi_i)^2 + d_i^2 \cos^2\phi_i\big)^{-1/2}$, it can be shown (see Theorem 1 in [5]) that for any robot $\mathbf{R}_i$ which is in (d_i, ϕ_i)-formation at time $t = 0$ and $\arcsin(K_0^- d_i \cos\phi_i) \leq \theta_0(0) \leq \arcsin(K_0^+ d_i \cos\phi_i)$, with controls,

$$v_i = v_0\, \frac{\cos(\theta_0 - \phi_i)}{\cos\phi_i}\,, \quad \omega_i = v_0\, \frac{\sin\theta_0}{d_i \cos\phi_i}, \tag{6}$$

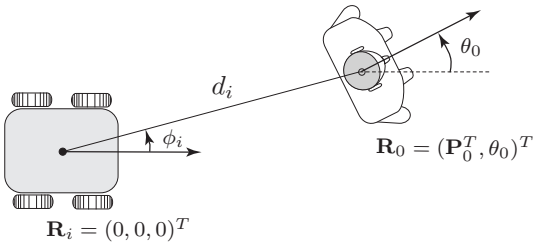

Fig. 2. The leader $\mathbf{R}_0$ and follower $\mathbf{R}_i$, $i \in \{1, \ldots, N\}$ are in (d_i, ϕ_i)-formation. Differently from [5], the pose of the leader, which is a human in this paper, is expressed in the follower's reference frame.

then $\mathbf{R}_0$ and $\mathbf{R}_i$ are in (d_i, ϕ_i)-formation and $\forall\, t \geq 0$, $\arcsin(K_0^- d_i \cos\phi_i) \leq \theta_0(t) \leq \arcsin(K_0^+ d_i \cos\phi_i)$. Geometrically speaking, this means that $\mathbf{R}_i$ lies in an arc of circle centered at the leader with orientation $\theta_0 + \phi + \pi$ and aperture $\arcsin(K_0^+ d_i \cos\phi_i) - \arcsin(K_0^- d_i \cos\phi_i)$ at all times (see Fig. 2 in [5]). In this respect, the formations considered in this paper have the special property of being *non-rigid* [20].

Let us now address the problem of *stabilizing* the leader-follower formation (i.e., we assume here that the robots are *not* initially in formation). Let $\mathbf{R}_0$ be the formation leader satisfying the trajectory constraint (V_0, K_0^-, K_0^+). If conditions (4) and (5) hold, and (see Theorem 2 in [5]),

$$0 < W_0 \leq v_0(t), \tag{7}$$

then for each follower $\mathbf{R}_i$ there is $\bar{\epsilon} > 0$ such that for any $\epsilon : 0 < \epsilon < \bar{\epsilon}$, there exist suitable controls v_i, ω_i,

$$v_i(t) = \begin{cases} V_p, & \text{if} \quad \theta_0(t) \notin \Gamma_\epsilon, \\ \frac{v_0(t)\cos(\theta_0(t)-\phi_i)+\eta_i(t)\,\langle \mathbf{E}_i(t), \boldsymbol{\tau}(\phi_i)\rangle}{\cos\phi_i}, & \\ & \text{if} \quad \theta_0(t) \in \Gamma_\epsilon, \end{cases} \tag{8}$$

$$\omega_i(t) = \begin{cases} V_p\, K_p^+, & \text{if } \ \theta_0(t) \notin \Gamma_\epsilon \ \text{ and } \ K_p^+ \geq 0, \\ V_p\, K_p^-, & \text{if } \ \theta_0(t) \notin \Gamma_\epsilon \ \text{ and } \ K_p^+ < 0, \\ \frac{v_0(t)\sin(\theta_0(t)+\eta_i(t)\,\langle \mathbf{E}_i(t), \boldsymbol{\nu}(0)\rangle}{d_i \cos\phi_i}\ , & \text{if } \ \theta_0(t) \in \Gamma_\epsilon, \end{cases} \tag{9}$$

where $\Gamma_\epsilon = \{x \in \mathcal{S}^1 | (K_0^- - \epsilon)\, d_i \cos\phi_i \leq \sin x \leq (K_0^+ + \epsilon)\, d_i \cos\phi_i\}$, $\mathbf{E}_i(t)$ is defined in (3), $\langle \cdot, \cdot \rangle$ denotes the scalar product and $\eta_i(t)$ is given by

$$\eta_i(t) = \min\Big(\frac{(v_0 - W_0/2)\cos(\theta_0 - \phi_i)}{|\langle \mathbf{E}_i(t),\, \boldsymbol{\tau}(\phi_i)\rangle|}\,, \frac{[\min((K_0^+ + \epsilon/2 - \kappa_0), (\kappa_0 - (K_0^- - \epsilon/2))]\, d_i \cos\phi_i}{|\langle \mathbf{E}_i(t),\, \boldsymbol{\nu}(0)\rangle|}\,, \frac{V_p \cos\phi_i - v_0 \cos(\theta_0 - \phi_i)}{|\langle \mathbf{E}_i(t),\, \boldsymbol{\tau}(\phi_i)\rangle|}\,, v_0 \frac{K_p^+ d_i \cos(\theta_0 - \phi_i) - \sin\theta_0}{|\langle \mathbf{E}_i(t),\, \boldsymbol{\nu}(0)\rangle| + |K_p^+||\langle \mathbf{E}_i(t),\, \boldsymbol{\tau}(\phi_i)\rangle|}\,, v_0 \frac{\sin\theta_0 - K_p^- d_i \cos(\theta_0 - \phi_i)}{|\langle \mathbf{E}_i(t),\, \boldsymbol{\nu}(0)\rangle| + |K_p^-||\langle \mathbf{E}_i(t),\, \boldsymbol{\tau}(\phi_i)\rangle|}, M\Big),$$

being $M > 0$ a gain constant (with the convention that $1/0 = +\infty$), such that $\mathbf{R}_0$ and $\mathbf{R}_i$ are asymptotically in (d_i, ϕ_i)-formation and $\exists\, \bar{t} \geq 0 : \forall\, t \geq \bar{t}$, $\arcsin((K_0^- - \epsilon)\ d_i \cos\phi_i) \leq \theta_0(t) \leq \arcsin((K_0^+ + \ \epsilon)\, d_i \cos\phi_i)$. Note that the stabilizing controller (8)-(9) allows the follower $\mathbf{R}_i$ to be asymptotically in (d_i, ϕ_i)-formation if the leader $\mathbf{R}_0$ satisfies the inequalities (4), (5) and (7), and that the positive constant W_0 in (7) is used to keep $v_0(t)$ away from zero. The control strategy essentially consists of two steps: in the first step $\mathbf{R}_i$ moves with maximal linear and angular velocities until its direction is sufficiently close to that of the leader, while in the second step $\mathbf{R}_i$ uses (6) with an added stabilizing term in order to reduce the error asymptotically to zero. As it will become clearer in the next section, in our setup each follower is able to locally compute its control law by only relying on the information provided by its on-board sensor.

In order to avoid possible *collisions* between the followers, inspired by [21] let us define,

$$(v_i(t),\, \omega_i(t))^T \;=\; \big(V_p,\, -\lambda \sum_j \dot{\vartheta}_{j,\,\mathrm{A}}\big)^T, \tag{10}$$

if j is such that $\|({}^i x_j, {}^i y_j)^T\| \leq r_d$ and set $v_i(t)$, $\omega_i(t)$ as in (8), (9) if $\|({}^i x_j, {}^i y_j)^T\| > r_d$, $\forall\, j \neq i$, where $\vartheta_{j,\,\mathrm{A}} \triangleq \mathrm{atan2}({}^i y_j, {}^i x_j)$ with $({}^i x_j(t), {}^i y_j(t))^T$ the position of robot $\mathbf{R}_j$ in the reference frame of robot $\mathbf{R}_i$ at time t, λ is a positive gain, and r_d is the radius of the collision avoidance disk centered at $\mathbf{R}_i$. In other words, if all the other followers are outside its collision avoidance disk, robot $\mathbf{R}_i$ applies the standard stabilizing control and formation maintenance has the highest priority: otherwise, it adjusts its angular velocity according to the position of the follower(s) $\mathbf{R}_j$ inside its avoidance disk and keeps its forward velocity constant.

Notice that Eq. (4)-(5), (7) introduce a useful *mapping* between the constraints of the N robots and the bounds on the linear velocity and curvature of the leader. In fact, each robot has constraints which are related to its formation parameters $(d_i,\, \phi_i)$ and to its mechanical limitations $(V_p,\, K_p^-,\, K_p^+)$. If we consider a formation of N robots, it would be impractical and confusing for the user to receive haptic stimuli which notify the violation of each constraint of the N robots. The proposed mathematical formulation tries to "compress" as much as possible the information relative to the constraints of each robot without prejudicing too much the level of informativeness. Our mapping between the constraints of the N robots and the bounds on velocities of the leader allows us to use simple haptic stimuli which must elicit three basic behaviors: turn left, turn right and slow down.

In the next section we will present our visual human-detection mechanism, and in Sect. 4 we will show how vibrotactile signals produced by a haptic bracelet can be used to correct the trajectory of the leader according to the formation specifics.

3 Visual Detection and Tracking of the Leader

This section provides an overview of the major steps of our method for detecting the human leader from the visual information provided by the RGB-D cameras onboard the follower robots. In what follows, we will assume that the robot xy-plane is parallel to the floor. As a preliminary step, we perform an extrinsic calibration of the RGB-D camera and robot reference frames. The homogeneous matrix $\mathbf{H}_{\mathcal{K}}^{\mathcal{R}}$, that relates the robot frame ($\mathcal{R}$) with the camera frame ($\mathcal{K}$), is estimated using a custom algorithm derived from [22]. The main motivation for this preliminary step is that the formation control strategy described in Sect. 2 is computed with respect to the robots' center, so it is necessary to express the input data in the robots'

(a) (b) (c) (d)

Fig. 3. *Human-body detection method on real data.* (a) The initial point cloud is downsampled, and expressed in the robot frame. (b) Data points which lie outside a given box are removed, while the remaining points are projected onto the robot xy-plane, and a clustering filter is applied (c). The position and orientation of the human body is detected through ellipse fitting (d).

frames. Given an input point cloud of the scene, we first downsample the data using a voxel grid filter with a leaf size of 2 cm (see Fig. 3(a)). We then express the downsampled point cloud $\mathbf{P}^{\mathcal{K}}$ in the robot reference frame using the estimated homogeneous matrix $\mathbf{P}^{\mathcal{R}} = \mathbf{H}^{\mathcal{R}}_{\mathcal{K}}\,\mathbf{P}^{\mathcal{K}}$ where $\mathbf{P}^{\mathcal{R}}$ represents the scene points in the robot frame. We discard all points that lie outside a given bounding box (Fig. 3(b)). As previously mentioned in [3], [4], since the shoulders can be considered as a sort of steering wheel that drives the human body with a delay of 0.2 s, in the detection phase we are mainly interested in recognizing the *human torso*. In this regard, we discard all the points which lie below the hip of the subject. We then project the points onto the robot xy-plane, and perform a cluster filtering discarding those clusters whose dimension is outside a given range (Fig. 3(c)). Finally, an ellipse fitting is performed over the clusters. We consider the human body as the cluster that best fits the ellipse, having the origin of the reference frame coincident with the ellipse center (Fig. 3(d)). Using this approach, the range in which the person can be detected and tracked is approximately between 0.8 m and 5.3 m in front of the Kinect.

Note that once the human body has been identified in the initial frame, to facilitate the human tracking in the successive frames, the bounding box can be updated (in terms of orientation, position and dimension) in order to define a proper region centered at the person. The proposed approach is robust to interferences in the depth image caused by multiple RGB-D devices observing the same scene.

4 Haptic Feedback

In this section, we describe the main features of our haptic bracelet and the nature of the vibrotactile feedback provided to the human. We also present the results of an experimental study that we conducted to assess how the stimuli produced by the bracelet are perceived by humans.

4.1 Description of the haptic bracelet

Studies have demonstrated that vibration is best on hairy skin due to skin thickness and nerve depth, and that vibrotactile stimuli are best detected in bony areas [23]. In particular, wrists and spine are generally preferred for detecting vibrations, with arms next in line [24], [25]. Movement can decrease detection rate, and increases response time of particular body areas [26]. For example, walking affects lower body sites the most [25].

Since in our setup the haptic feedback will provide the leader with information about the constraints on her/his linear and angular velocities, three vibrating motors are utilized to independently warn the user. Recent studies have demonstrated that a bracelet shape with three vibrating motors circling the forearm ensures sufficient distance between the motors while covering a minimal forearm area [16]. In fact, the minimal distance between two stimuli to be differentiated is about 35 mm on the forearms: in two-point discrimination perception there is no evidence for differences among the left and right sides of the body, and women are known to be more sensitive than men to skin stimulation [23], [27]. Following these guidelines, we designed a wearable haptic bracelet in which three cylindrical vibro-motors, L (left), C (center) and R (right) are independently controlled via an external PC using the Bluetooth communication protocol: the motors generate vibratory signals to warn the human of potential violations of formation constraints (see Fig. 4). The communication is realized with an RN42 Bluetooth module connected to an Arduino mini pro 3.3 V with a baud rate of 9600. An Atmega 328 microcontroller installed on the Arduino board is used to independently control the vibration amplitude of each motor. Although tactile stimulations under 100 Hz improve the spatial resolution of the vibration's perception [28], the maximal sensitivity is achieved around 200-300 Hz [29] (the human perceptibility range is between 20 and 400 Hz). Three Precision Microdrives 303-100 Pico Vibe 3.2 mm vibration motors were placed into three fabric pockets on the external surface of the bracelet (the width of the wristband is about 60 mm), with shafts aligned with the elbow bone. Since the rotating masses are exposed, we placed each motor inside a cylindrical case of ABS plastic in order to protect

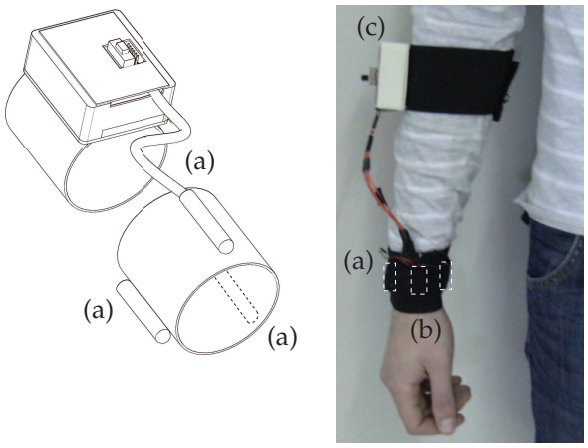

Fig. 4. Human-robot interaction is achieved via a vibrotactile bracelet equipped with three vibrating motors, (a), attached to an elastic wristband (b). The Li-Ion battery and the Arduino board are in (c).

them from damage and guarantee a correct operation. The motors have a vibration frequency range of 100-280 Hz and a vibration amplitude of 0.6 g with a 100 gram inertial test load at rated voltage of 3 V, where $\mathrm{g} = 9.81\ \mathrm{m/s^2}$. Although more sophisticated bracelets have been recently proposed in the literature (see for example [30]), our goal was to design an inexpensive and mechanically simple device capable of producing easily-reproducible results.

4.2 Generation of the vibrotactile feedback

Our vibrotactile feedback simply consists in activating the vibro-motors when the formation constraints are about to be violated (with a given threshold), and in increasing the vibration frequency proportionally to the constraint violation (increasing intensity improves the detection rate and reduces the reaction time [25]). A repulsive haptic-feedback mechanism was adopted. A special case occurs when a robot performs an evasive maneuver (Eq. (10)) in order to avoid collisions with the other followers: since the robot does not use the stabilizing formation control law, its contribution will not be considered in the notification of formation-constraint violation.

Let f_m, f_M be the minimal and maximal vibration frequency of each motor, respectively, and $f_j(t)$ the vibration frequency of motor $j \in \{L, C, R\}$ at time t. As discussed in Sect. 2, the leader should respect both velocity and curvature constraints. The curvature constraints involve the activation of motors L and R in the bracelet, while the velocity constraints are displayed through motor C. The curvature of the path followed by the leader at time t is $\kappa_0(t) = \omega_0(t)/v_0(t)$ with $v_0(t) > 0$. Substituting (2) in (4) and introducing the curvature threshold $\alpha_c \in \mathbb{R}_{>0}$, we obtain the following curvature constraints for each follower $\mathbf{R}_i$, $i \in \{1, \ldots, N\}$ ($d_i > 0$, $\phi_i : |\phi_i| < \pi/2$, cf. Sect. 2), $-\frac{1}{d_i} < -\frac{1}{d_i} + \alpha_c \leq \kappa_0(t) \leq \frac{1}{d_i \cos\phi_i} - \alpha_c < \frac{1}{d_i \cos\phi_i}$, if $\phi_i \geq 0$ and $-\frac{1}{d_i \cos\phi_i} < -\frac{1}{d_i \cos\phi_i} + \alpha_c \leq \kappa_0(t) \leq \frac{1}{d_i} - \alpha_c < \frac{1}{d_i}$, if $\phi_i < 0$. These constraints can be combined to yield the following *formation curvature constraints*,

$$\begin{aligned} &\max_i(-\tfrac{1}{d_i} + \alpha_c) \leq \kappa_0(t) \leq \min_i(\tfrac{1}{d_i \cos\phi_i} - \alpha_c), \text{ if } \phi_i \geq 0, \\ &\max_i(-\tfrac{1}{d_i \cos\phi_i} + \alpha_c) \leq \kappa_0(t) \leq \min_i(\tfrac{1}{d_i} - \alpha_c), \text{ if } \phi_i < 0. \end{aligned} \tag{11}$$

This means that in the case that two or more violations of the same constraint are simultaneously detected, a vibrational signal corresponding to the constraint which is violated the most is generated.
Let $\delta^+(t)$, $\delta^-(t)$ be the amount of violation of the given constraints at time t, when $\omega_0(t)$ is positive or negative, respectively. From (11) we obtain,

$$\delta^+(t) = \begin{cases} \kappa_0(t) - \min_i(\frac{1}{d_i \cos\phi_i} - \alpha_c), & \text{if } \phi_i \geq 0, \\ \kappa_0(t) - \min_i(\frac{1}{d_i} - \alpha_c), & \text{if } \phi_i < 0, \end{cases}$$

$$\delta^-(t) = \begin{cases} \max_i(-\frac{1}{d_i} + \alpha_c) - \kappa_0(t), & \text{if } \phi_i \geq 0, \\ \max_i(-\frac{1}{d_i \cos\phi_i} + \alpha_c) - \kappa_0(t), & \text{if } \phi_i < 0. \end{cases}$$

If $\max(\delta^+(t), \delta^-(t)) \geq 0$, the human is about to violate the curvature constraints and hence the following vibrational feedback is generated by the motors,

$$f_j(t) = (f_M - f_m)\frac{\max(\delta^+(t), \delta^-(t))}{\alpha_c} + f_m, \tag{12}$$

with $j = L$ if $\delta^+(t) \geq 0$ and $j = R$ if $\delta^-(t) \geq 0$. As far as the linear velocity of the human leader is concerned, from (1), (7) and introducing a velocity threshold value $\alpha_l \in \mathbb{R}_{>0}$, we obtain that $v_0(t)$ should fulfill the following constraint,

$$0 < W_0 < v_0(t) < V_0 - \alpha_l < V_0, \tag{13}$$

where V_0 satisfies equation (5) for each follower $\mathbf{R}_i$. If the leader is moving too fast, i.e., $v_0(t) \geq V_0 - \alpha_l$, the amount of constraint violation is $\beta^+(t) = v_0(t) - V_0 + \alpha_l$, and a vibration with the following frequency is generated by motor C:

$$f_C(t) = (f_M - f_m)\frac{\beta^+(t)}{\alpha_l} + f_m. \tag{14}$$

Note that constraint (13) also specifies a lower bound W_0 for the linear velocity $v_0(t)$. However, W_0 can be set arbitrarily small so that this bound is never violated in practice.

Remark 1: Since $v_0(t) > 0$, the constraint on the curvature can be considered as a constraint on the angular velocity. In fact from (11) we obtain $v_0(t)\max_i(-\frac{1}{d_i} + \alpha_c) \leq \omega_0(t) \leq v_0(t)\min_i(\frac{1}{d_i \cos\phi_i} - \alpha_c)$, if $\phi_i \geq 0$, and $v_0(t)\max_i(-\frac{1}{d_i \cos\phi_i} + \alpha_c) \leq \omega_0(t) \leq v_0(t)\min_i(\frac{1}{d_i} - \alpha_c)$, if $\phi_i < 0$. Since (13) represents a constraint on the linear velocity, when the curvature constraint (11) is violated a vibrational feedback is

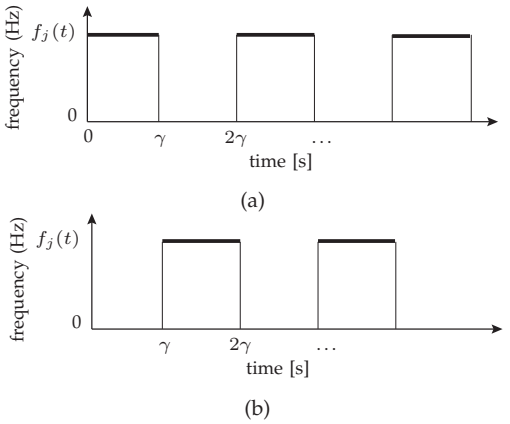

Fig. 5. *Temporization of the stimuli.* In order to avoid the aftereffect problem, a periodic vibrational pattern with period 2γ is displayed to the user (a). To keep signal recognition simple in the case of a combination of stimuli, we alternate the patterns in (a) and (b).

sent to the user in order to warn her/him about her/his angular velocity. ◇

Note that the leader can perceive an imminent violation of the formation's constraints (see Eq. (11), (13)), but she/he is completely unaware of the identity or number of followers which are responsible for the occurrence of this event. In this sense our human-robot interaction mechanism is invariant to the cardinality of the followers and thus fully scalable.

Referring to equations (12)-(14), in order to reduce the *aftereffect* problem (vibration effects usually persist after the end of the stimulation, see [31] and the references therein), we displayed a periodic vibrational pattern with period 2γ instead of a continuous signal (see Fig. 5(a)). Moreover, to keep signal recognition as simple as possible, we did not consider superpositions of two signals. In case of a combination of stimuli, we alternated two patterns (cf. Fig. 5(a)-(b)). It is worth noting that we avoided cases in which all motors were turned on, and cases in which the left and right motors were simultaneously activated, since they never occur in our leader-follower team.

Since a team generally includes more than one follower, a suitable communication policy should be adopted for our haptic bracelet. In order to maintain a proper temporization of the vibrational pattern, and because of the limited one-to-one communication capabilities of our Arduino-based haptic bracelet, only one robot is in charge of *directly* communicating with the haptic device. This gateway robot receives the information of possible violations of formation constraints from all the other followers, and in the case that two or more violations of the same constraint are simultaneously detected, it generates a vibrational signal corresponding to the constraint which is violated the most. Depending on the adopted technology, more sophisticated communication mechanisms will be explored in future works.

4.3 Evaluation of the haptic bracelet

This section focuses on how the stimuli generated by the proposed bracelet are perceived by humans. Because a great deal of psychophysical literature already exists on the fundamental topic of how humans interpret vibrational stimuli, e.g., [32], [33], we tailored the design of our study to match the device's capabilities and the scenario in which we envision it being used.

4.3.1 Subjects

The proposed device has been tested on 14 healthy subjects (12 males, age range 22-56, 12 right-handed). 9 of them had tried previous prototypes of our bracelet, whose working principles, however, were significantly different (cf. [8]): we did not notice any evident discrepancy between the performance of these 9 subjects and the remaining 5. None of the participants reported any deficiency in the perception abilities (vision, hearing, touch and proprioception).

4.3.2 Methods and results

We performed two different experiments. In the first one, a single signal (center C, left L, right R) or a combination of signals (center-left CL, center-right CR) at different vibrational frequencies was sent to the haptic bracelet. The subjects were asked to recognize the source of the stimulus (i.e., they had to identify which motors were vibrating). Every signal was presented six times in a pseudo-randomized order with pseudo-random frequency. In the second experiment we evaluated the minimal frequency variation that can be discriminated using the proposed bracelet. In this case, a pseudo-random signal with pseudo-random frequency was presented to the users. Subsequently, the same signal but with a different frequency was delivered. In case of a combination of stimuli, the frequency variation was randomly applied to one signal only. The subjects were asked to determine if the second stimulus had a higher (or lower) frequency than the first one. This experiment was instrumental in determining a suitable frequency variation which allowed the users to identify the level of violation of a particular constraint. All participants were informed about the adopted procedure before the beginning of each experiment, and a five-minute familiarization period was given to each subject. In both the experiments the subjects took a small break after each evaluation set. During all trials, participants wore headphones reproducing white noise to eliminate auditory cues from the device. Each subject wore the device on the wrist of her/his dominant hand. The evaluation set was composed of two sets of 30 trials each. The range of frequencies was 130-280 Hz (amplitude range 0.28-0.6 g), where the minimal perceptible vibrational frequency/amplitude was determined using the classical staircase method [34]. Note that the vibrating motors were controlled by applying a certain voltage which determined changes in both frequency and amplitude of the vibrotactile signal.

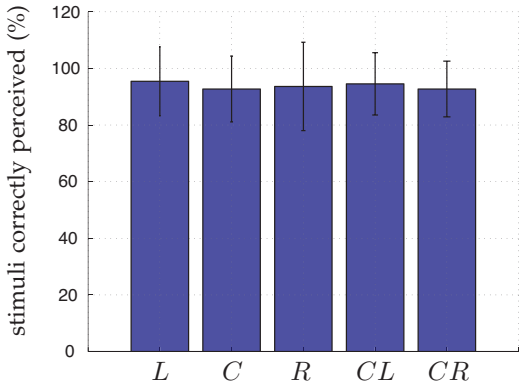

Fig. 6. Mean and standard deviation of the stimuli (L, C, R, CL, CR) correctly perceived by the users.

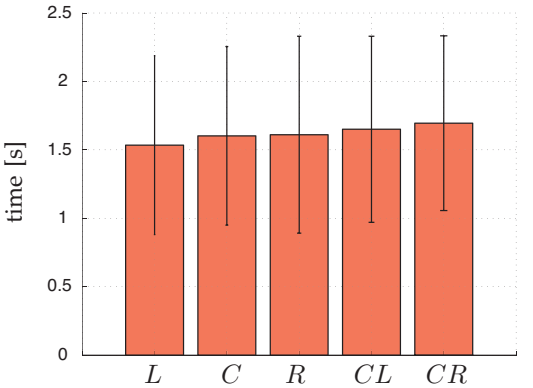

Fig. 7. Mean and standard deviation of the time the users needed to correctly recognize a given haptic stimulus (L, C, R, CL, CR).

Within a trial, we repeated the stimuli until the subjects were able to give a correct/wrong answer, with a maximum limit of 6 repetitions.

In the first experiment, the users could correctly perceive and distinguish the majority of the proposed stimuli (see Fig. 6). An in-depth analysis revealed that in the presence of a combination of signals with a big disparity in the vibrational frequency, the subjects could correctly perceive at least one of the two involved stimuli, usually the most intense. In the human-robot formation setup of this paper, this means that the leader is able to perceive the vibrotactile feedback relative to the constraint that is violated the most. Mean and standard deviation of the time elapsed to perceive the stimuli are reported in Fig. 7.

In order to evaluate the statistical significance of the differences between stimuli, we performed a repeated-measures ANOVA [35] on the observed number of correct responses (ANOVA analyzes the groups variances to test the heterogeneity of their means). To that end, we first computed the proportion of correct responses for each subject in relation to the type of stimulus. Then, we used the $\arcsin(\sqrt{(\cdot)})$ transformation to stabilize the variance of the computed proportions. Finally, we took into account possible violation of the sphericity condition by using Greenhouse-Geissers epsilon to adjust the degrees of freedom of the ANOVA. If the p-value is below our significance level $\zeta = 0.05$, we rejected the null hypothesis that all the means of the different groups are the same. Results showed the type of stimulus (L, C, R, CL, CR) did not significantly influence the percentage of correct responses, indicating that the subjects were not more likely to respond correctly when one or the other type of stimulus was provided, $F(4, 52)=1.236$. A repeated-measures ANOVA on the elapsed time was also performed. Results revealed that the stimulus type did not significantly influence the time elapsed to perceive it, $F(2.170, 28.207) = 3.057$. In the second experiment, in order to make frequency an effective means of differentiation between stimuli, we considered differences of more than $\pm 20\%$ in intensity change [23]. In particular, we used the following frequency variations: $\pm 20\%$, $\pm 25\%$, $\pm 30\%$, $\pm 35\%$, $\pm 40\%$. Fig. 8 shows the mean and standard deviation of the percentage of frequency variations correctly perceived. We chose a minimal variation of $\pm 30\%$ of the signal, since it is the minimal variation that guarantees 80% correct perceptions. Such a choice resulted in a maximum of 3 dynamic frequency changes within the 130-280 Hz interval (this is consistent with [23] where it was suggested to limit the number of different frequencies to fewer than 7, with a number of dynamic changes smaller than 4).

5 Experimental Validation

5.1 Numerical tests

Computer simulations have been performed to test the effectiveness of our formation control law and haptic-feedback generation mechanism. In our first test, we considered a team consisting of a leader and two follower robots. In order to study the robustness of the *stabilizing* formation control strategy (8)-(9), the position and orientation of the leader was

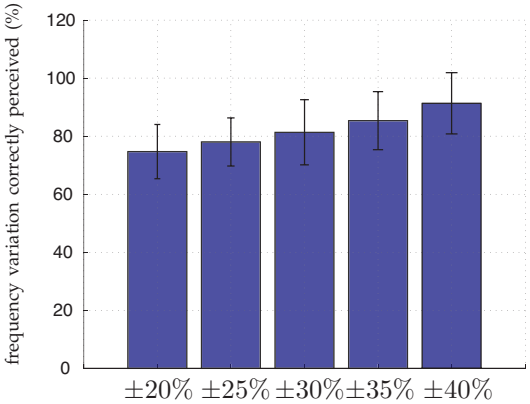

Fig. 8. Mean and standard deviation of the frequency variations correctly perceived by the users.

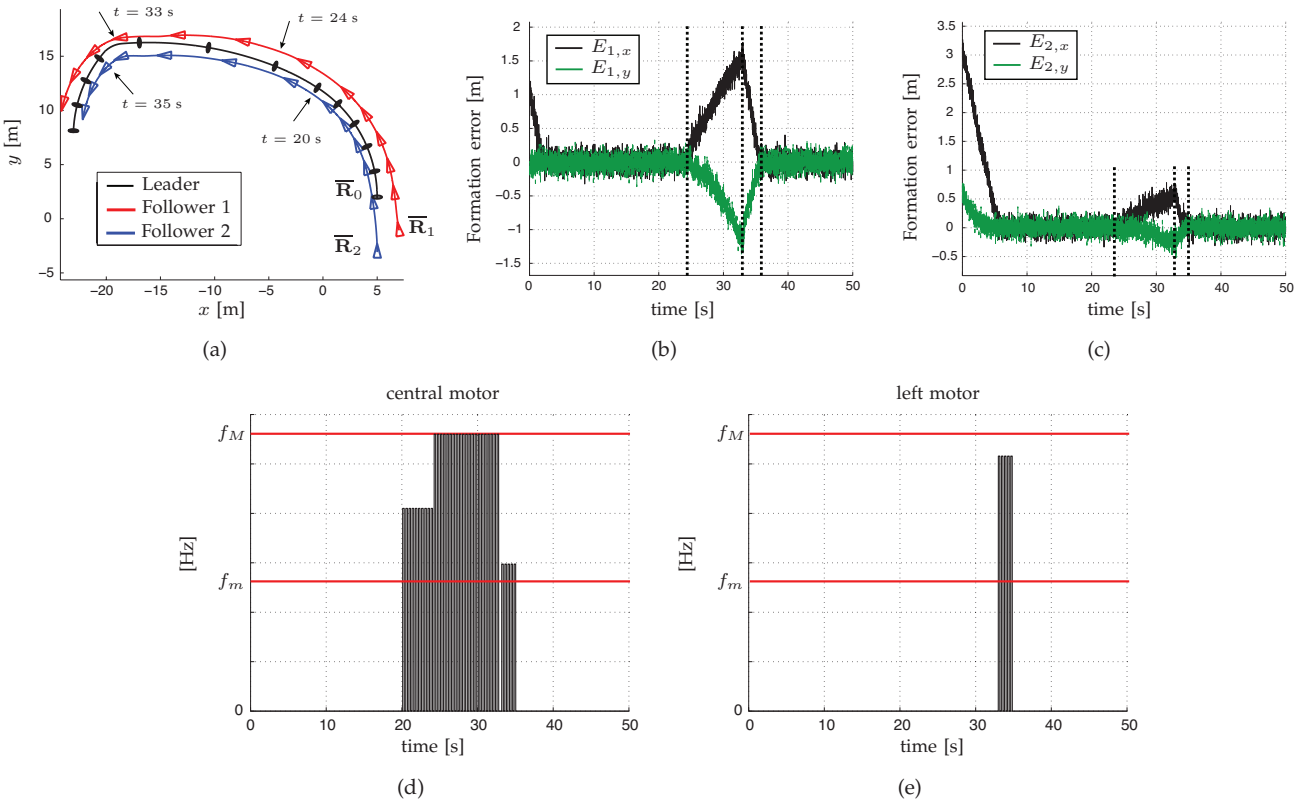

Fig. 9. *Simulation results:* (a) Trajectory of the leader (black) and followers; (b), (c), time evolution of the formation errors $\mathbf{E}_1 = (E_{1,x}, E_{1,y})^T$ and $\mathbf{E}_2 = (E_{2,x}, E_{2,y})^T$ of the two followers; (d), (e) vibrational frequencies of the central and left motor of the bracelet.

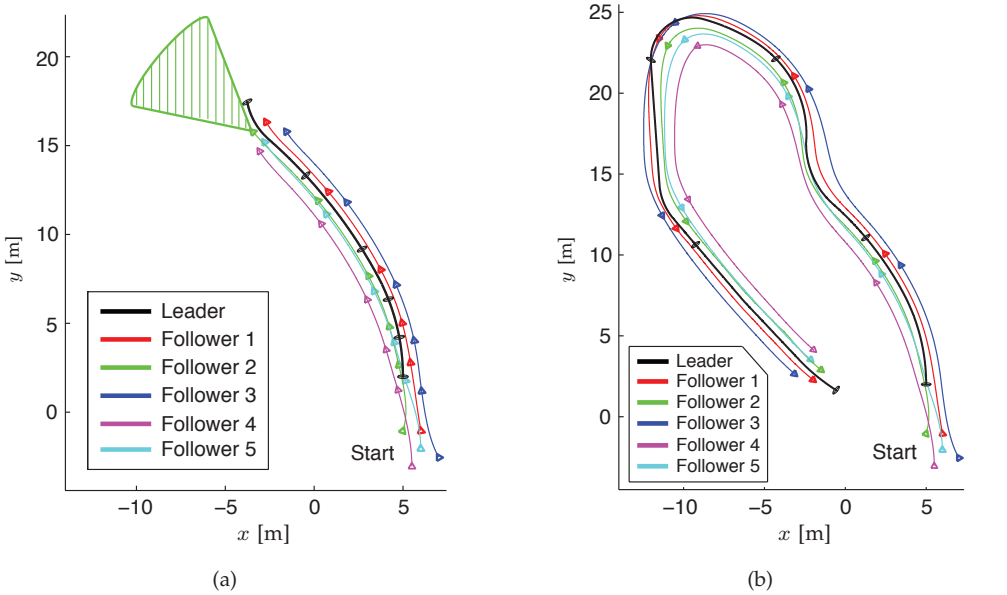

Fig. 10. *Simulation results (multiple followers)*: Trajectory of the leader (black) and of five followers, (a) without haptic feedback, and (b) with haptic feedback.

corrupted with zero-mean white Gaussian noise with standard deviation 0.1 m and 10 deg., respectively. Table 1 reports the initial conditions of the leader and followers, and the formation, controller and vibrotactile-feedback parameters. The leader's velocity $(v_0(t), \omega_0(t))^T$ is $(0.6, 0.05)^T$ if $t \in [0, 20) \cup [35, 50]$, $(1, 0.05)^T$, if $t \in [20, 24)$, $(1.6, 0.05)^T$, if $t \in [24, 33)$, and $(0.85, 0.4)^T$, if $t \in [33, 35)$, where time is in seconds. For the sake of simplicity we did not simulate the reaction of the human to the haptic feedback. The vibra-

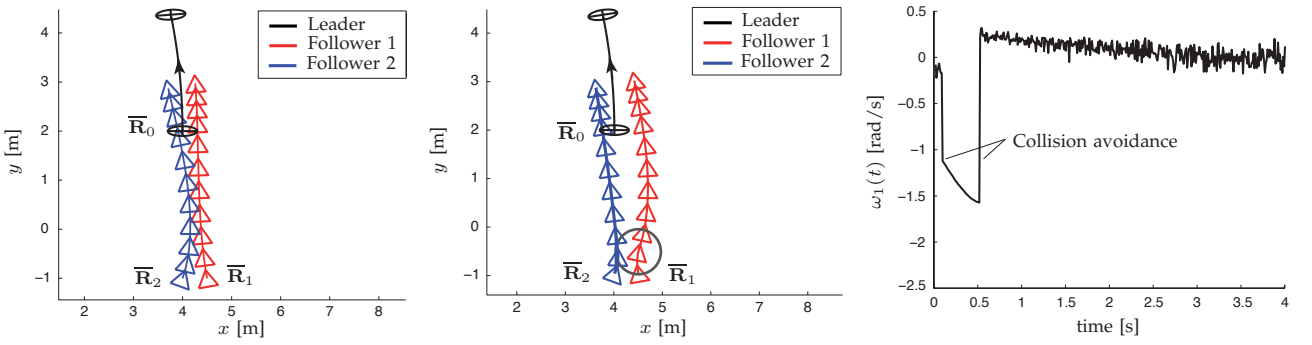

Fig. 11. *Simulation results (collision avoidance)*: Trajectory of the leader (black) and two followers, (a) without, and (b) with collision avoidance (the collision avoidance disk of $\mathbf{R}_1$ is shown in grey, and the robots are displayed every 0.4 s); (c) Time evolution of the angular velocity $\omega_1(t)$ of follower $\mathbf{R}_1$ according to (10).

tional frequencies of the central and left motor of the bracelet reported in Figs. 9(d)-(e) show how violations of formation constraints are translated into suitable vibrotactile patterns. Fig. 9(a) reports the trajectory of the leader and followers. At the beginning the leader's velocity satisfies the formation constraints. When $t = 20$ s, the linear velocity of the leader increases ($V_0 - \alpha_l < v_0(t) < V_0$) and a proper signal is sent to the central motor of the bracelet. Since the constraint is not violated, the followers are still able to keep the formation. At time $t = 24$ s the formation constraint is violated ($v_0(t) > V_0$), and a signal with maximal vibrational frequency is generated by the central motor. Since the constraint is violated, the followers are unable to follow the leader, and the formation errors for the first ($\mathbf{E}_1$) and second follower ($\mathbf{E}_2$) increase (see Figs. 9(b)-(c)). When $t = 33$ s the linear velocity of the leader decreases ($V_0 - \alpha_l < v_0(t) < V_0$) while the angular velocity increases, so that the violation of the curvature constraint in (11) is imminent. In this case the vibrational patterns in the central and left motor are alternated as mentioned in Sect. 4.2. Since no formation constraint is violated, the followers are able to reduce the formation error and achieve the desired formation.

Fig. 10 shows the performance of our control strategy when five followers are considered and the leader moves along a more involved trajectory: $(v_0(t), \omega_0(t))^T$ is $(0.6, 0.05)^T$, if $t \in [0, 10)$, $(1.4, 0.05)^T$, if $t \in [10, 17)$, $(1.5, -0.4)^T$, if $t \in [17, 21)$, $(0.9, 0.3)^T$, if $t \in [21, 30)$, $(0.6, 0.05)^T$, if $t \in [30, 35)$, $(0.9, 0.5)^T$, if $t \in [35, 41)$, $(1.2, 0)^T$, if $t \in [41, 50)$, $(1, 0.4)^T$, if $t \in [50, 54)$, $(1.6, 0)^T$, if $t \in [54, 60)$ and $(1.8, 0)^T$, if $t \in [60, 65]$. The formation parameters are, in this case, $d_1 = d_2 = 1.5$, $d_3 = 2.7$, $d_4 = 2.8$, $d_5 = 2.4$, $\phi_1 = \pi/12$, $\phi_2 = -\pi/12$, $\phi_3 = \pi/9$, $\phi_4 = -\pi/9$, $\phi_5 = -\pi/18$, and the other control and vibrotactile-feedback parameters are as those reported in Table 1, except for K_0^+ which is now 0.35. Similarly to the Kinect camera, we assumed that the sensor onboard the followers has an angular field-of-view (FOV) of 57 deg. horizontally and a range of 6 m. We implemented a simple "artificial intelligence" to the leader. The leader behaves as if she/he reacted to the haptic stimuli according to the statistical results reported in Figs. 6-7. Variations of the user's velocity due to these stimuli were modeled based on empirical estimations. In Fig. 10(a), the leader does not react to the haptic stimulation and by not respecting the formation constraints, she/he eventually exits from of the FOV of the second follower (shaded green in the figure). On the contrary, in Fig. 10(b) the leader responds to the stimuli of the haptic bracelet and she/he is able to adjust her/his velocity profile in order to maintain the trapezoidal formation.

$\overline{\mathbf{R}}_0$	$(5, 2, \pi/2)^T$
$\overline{\mathbf{R}}_1$	$(7, -1, 5\pi/9)^T$
$\overline{\mathbf{R}}_2$	$(5, -3, \pi/2)^T$
d_1, d_2 (m)	2.7, 2
ϕ_1, ϕ_2 (rad)	$7\pi/36$, $-\pi/10$
W_0, V_0, V_p (m/s)	0.05, 1.2, 1.5
K_0^-, K_0^+ (rad/m)	-0.35, 0.45
K_p^-, K_p^+ (rad/m)	-1, 1
ϵ, M (rad/m)	0.05, 3
α_l (m/s)	0.4
α_c (rad/m)	0.2
f_m, f_M (Hz)	130, 280

TABLE 1
Parameters used in the simulation of Fig. 9.

Finally, Fig. 11 illustrates the collision-avoidance strategy introduced in Sect. 2 with two followers. Here, $d_1 = d_2 = 1.5$, $\phi_1 = \pi/12$, $\phi_2 = -\pi/12$, $(v_0(t), \omega_0(t))^T = (0.6, 0.05)^T$ for all t, the radius of the collision avoidance disk is $r_d = 0.47$ m, and all the other control and haptic parameters are as those used in the previous simulation. Fig. 11(a) shows the trajectory of the leader and followers when collision avoidance is not enforced: in this case, the followers collide right after the beginning of the simulation. Fig. 11(b) shows that controller (10) with gain $\lambda = 1$, is able to effectively resolve the collision between the two followers. Fig. 11(c) finally reports the time evolution of the angular control $\omega_1(t)$ of the first follower

(cf. (10)): the spike in the figure corresponds to the activation of the collision-avoidance mode. Note that as in our first test, in Fig. 10 and Fig. 11 the position and orientation of the leader were corrupted with zero-mean white Gaussian noise.

To further corroborate the results of our numerical tests, in the next section we will present real-world experiments involving a human leader wearing our haptic bracelet and two wheeled robots.

5.2 Experiments

5.2.1 Subjects

14 healthy subjects were involved in our experiments (all of them participated in the evaluation of the bracelet, see Sect. 4.3.1). In order to evaluate the users' experience, at the end of the experiment we asked the subjects to answer a questionnaire using bipolar Likert-type seven-point scales. The questionnaire considered the comfort in using the proposed bracelet and its level of informativeness in reporting the formation constraints. An answer of 7 meant a very high comfort while an answer of 1 meant very low comfort. The questionnaire consisted of 8 questions.

5.2.2 Methods and results

The formation control strategy (8)-(9) has been tested in an indoor environment using two Pioneer P3AT robots equipped with a Microsoft's Kinect camera[1] (see Fig. 12). The motorized tilt of the camera was disabled during the experiments. A linear and a curvilinear trajectory have been considered for the human leader. We used the Point Cloud Library [36] to process the Kinect data, and extract the information about the human motion. The tracking algorithm ran at an average frame rate of 15 fps on a Mac Book with 4 GB RAM, 2.26 GHz Intel Core Duo CPU and an NVIDIA GeForce 9400M graphics card. Due to the actuation time of electric motors of the robots, the followers' velocities were computed every 0.2 s and sent to the robot via the TCP/IP protocol. The same time interval was used to send the haptic signals to the vibrotactile bracelet. In both the experiments, the followers were not initially in formation. They had to reach and keep it during the motion of the human leader. The followers' initial conditions with respect to the leader, and the parameters used in the tests are reported in Table 2. The value of V_0 was determined from the maximal translational velocity of the Pioneer P3AT robot. The minimal non-zero intensity change between two consecutive signals was set to $\pm 30\%$ of the signal (cf. Sect. 4.3). The above parameters have been chosen in order to maintain the person inside the FOV of the camera at all times. The first follower plays the role of gateway robot (cf. Sect. 4.2). In all the experiments, the subjects were asked to reach predefined checkpoints on a given trajectory, but no instructions were given about their linear and/or angular velocities. All subjects tried once without and once with haptic feedback. In Figs. 13-14, we report the results relative to follower $\mathbf{R}_1$ (in fact, the two robots exhibited very similar behaviors) and subject 1 (which is representative of our group of 14 people) for the linear and curvilinear trajectory, respectively. As far as the linear trajectory is concerned, if the haptic feedback is not provided and the leader does not satisfy the linear velocity constraint, the followers are unable to compensate for the initial formation error (see Fig. 13(b)). On the contrary, by using the vibrotactile bracelet, the user was able to easily adjust her/his velocities according to the provided feedback, and thus reach and keep the desired formation (see Fig. 13(c)). The corresponding vibrational frequency of the central motor is reported in Fig. 13(d).

In the second experiment the user had to satisfy constraints on both the linear and angular velocities. Again, the haptic feedback was crucial for reducing the formation error (see Figs. 14(b)-(c)). Figs. 14(d)-(e) report the vibrational frequencies of the central and left motors. Fig. 15 reports the mean and standard deviation of the Euclidean norm of the formation error $\mathbf{E}_1$ (obtained by averaging the errors over each time step along the entire trajectory, and over all the 14 subjects) for both the linear and curvilinear trajectories. As it is evident from the figure, the haptic feedback

Trajectory	linear	curvilinear
$\overline{\mathbf{R}}_1$	$(-2.6, 0, 0)^T$	$(-3, 1, -0.3491)^T$
$\overline{\mathbf{R}}_2$	$(-3, 2, -\pi/4)^T$	$(-3, -2, \pi/4)^T$
d_1, d_2 (m)	3, 2	2.5, 3.2
ϕ_1, ϕ_2 (rad)	0.3491, -0.2618	-0.3696, 0.2967
W_0, V_0, V_p (m/s)	0.05, 0.65, 0.7	0.05, 0.65, 0.7
K_0^-, K_0^+ (rad/m)	-0.3, 0.32	-0.3, 0.32
K_p^-, K_p^+ (rad/m)	-2, 2	-2, 2
ϵ, M (rad/m)	0.05, 2	0.05, 3
α_l (m/s)	0.15	0.15
α_c (rad/m)	0.14	0.14
f_m, f_M (Hz)	130, 280	130, 280

TABLE 2
Parameters used in the experiments.

1. Please notice that this paper is accompanied by multimedia material. The videos of the real-time experiments are available also at: http://goo.gl/K43Bg6

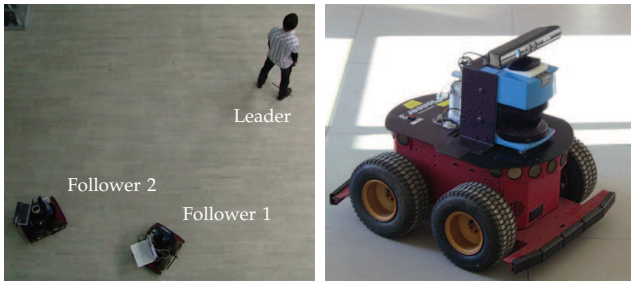

(a) (b)

Fig. 12. (a) Experimental setup; (b) Pioneer P3AT robot equipped with a Microsoft's Kinect camera.

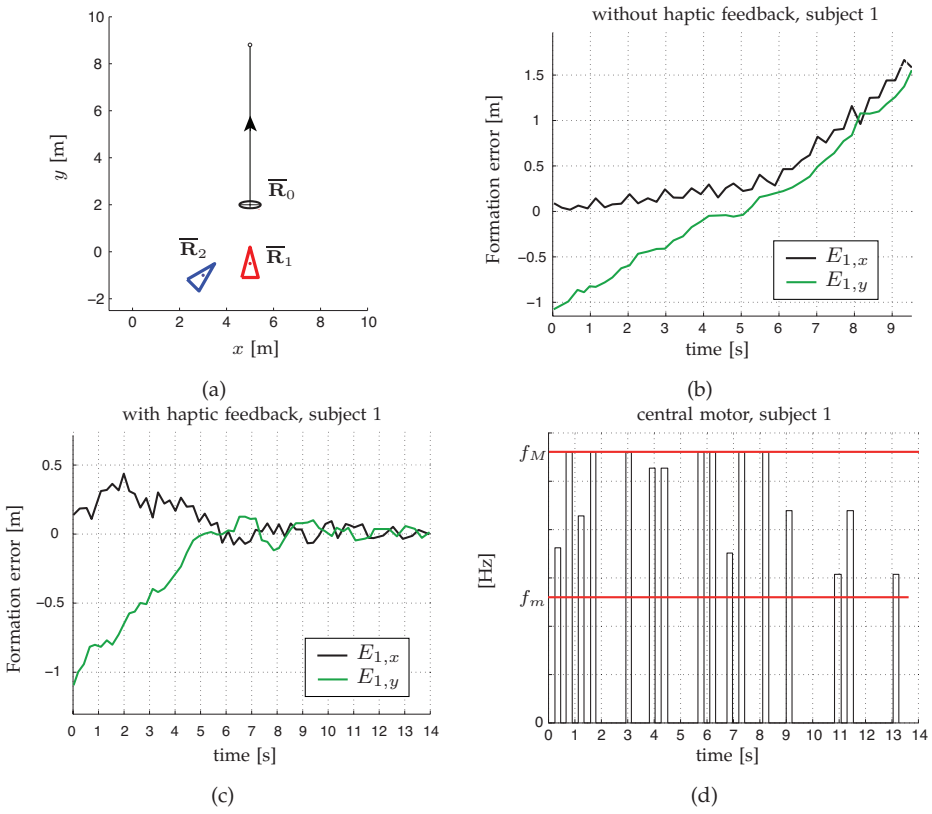

Fig. 13. *Experimental results for the linear trajectory.* (a) Initial disposition of the team members and planned leader trajectory (solid line); (b), (c) time evolution of the formation error $\mathbf{E}_1 = (E_{1,x}, E_{1,y})^T$ for subject 1 without and with haptic feedback; (d) vibrational frequency of the central motor of the bracelet.

plays a fundamental role in keeping the formation error small. The users' response at the end of the experiments was positive. In fact, according to our questionnaire, the mean value of the answers to the questions about the perceived comfort was 5.6, while it was 6.3 for the questions about the informativeness of the system.

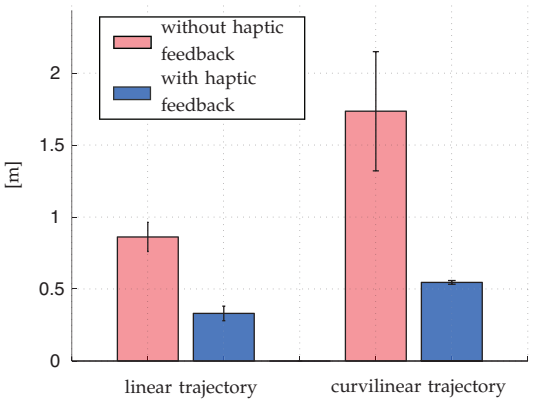

Fig. 15. Mean and standard deviation of $\|\mathbf{E}_1\|$ for both the linear and curvilinear trajectories. The values are obtained by averaging the errors over each time step along the entire trajectory, and over all the 14 subjects.

6 Conclusions and Future Work

In this paper we have presented a new formation control setup consisting of a human leader and multiple follower robots equipped with RGB-D sensors. Vibrotactile feedback provided by haptic bracelets is used to guide the human along trajectories that are feasible for the leader-follower formation. The effectiveness of the proposed designs has been demonstrated via numerical simulations and real-world experiments.

In future works, we aim at exploring alternative solutions for the generation of the vibrotactile feedback in order to make the system more reactive and informative to the user. We also plan to extend our results to teams including multiple humans and heterogeneous robots.

Acknowledgements

The research leading to these results has received funding from the European Union Seventh Framework Programme FP7/2007-2013 under grant agreement n. 601165 of the project "*WEARHAP - WEARable HAPtics for humans and robots*" and under grant agreement n. 288917 of the project "*DALi - Devices for Assisted Living*". The authors are grateful to C. Pacchierotti and L. Meli for useful discussions on the design of the psychophysical experiments, and to M. Aggravi for his support in the preparation of the experimental setup.

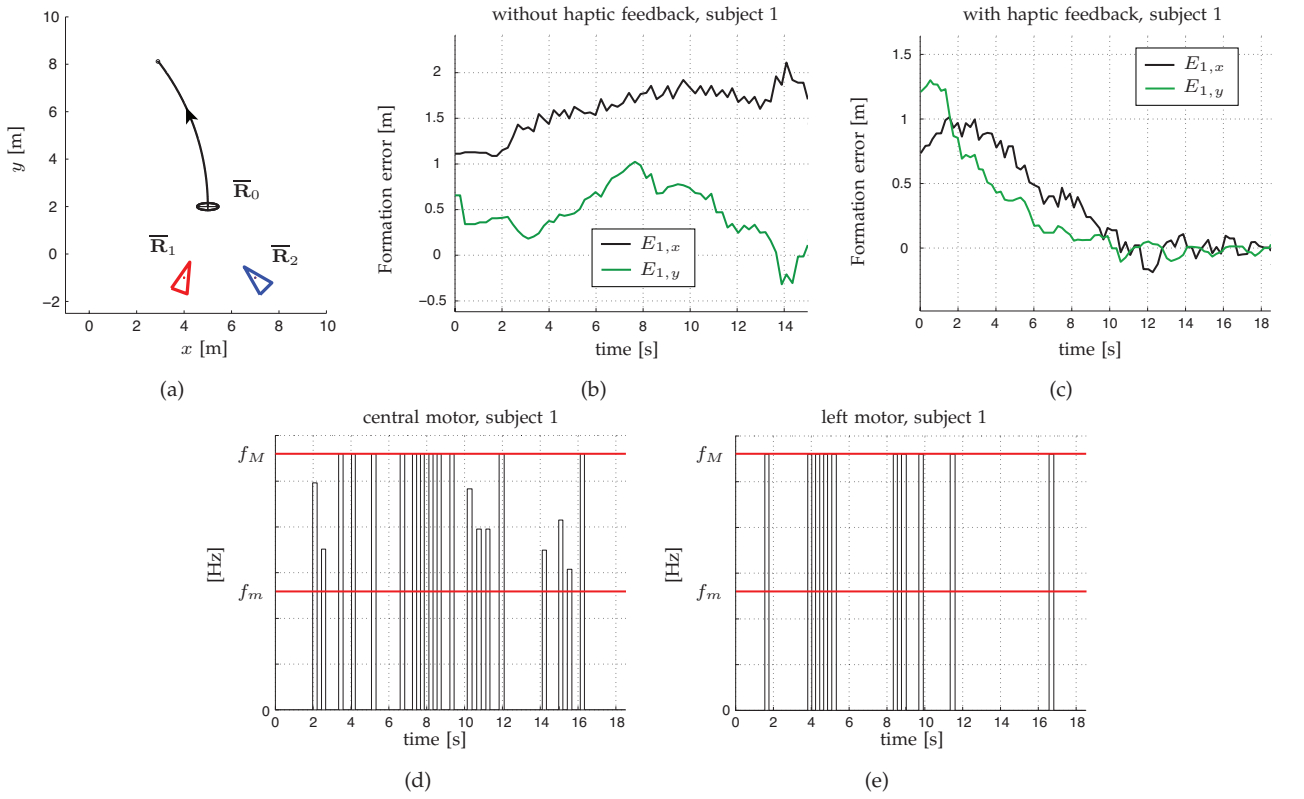

Fig. 14. *Experimental results for the curvilinear trajectory.* (a) Initial disposition of the team members and planned leader trajectory (solid line); (b), (c) time evolution of the formation error $\mathbf{E}_1 = (E_{1,x}, E_{1,y})^T$ for subject 1 without and with haptic feedback; (d), (e) vibrational frequencies of the central and left motor of the bracelet.

REFERENCES

[1] S. Thrun. Toward a framework for human-robot interaction. *Human-Computer Interaction*, 19(1-2):9–24, 2004.

[2] C. Ha and D. Lee. Vision-Based Teleoperation of Unmanned Aerial and Ground Vehicles. In *Proc. IEEE Int. Conf. Robot. Automat*, pages 1457–1462, 2013.

[3] G. Arechavaleta, J.P. Laumond, H. Hicheur, and A. Berthoz. On the nonholonomic nature of human locomotion. *Auton. Robot.*, 25(1):25–35, 2008.

[4] G. Arechavaleta, J.P. Laumond, H. Hicheur, and A. Berthoz. An optimality principle governing human walking. *IEEE Trans. Robot.*, 24(1):5–14, 2008.

[5] L. Consolini, F. Morbidi, D. Prattichizzo, and M. Tosques. Leader-follower formation control of nonholonomic mobile robots with input constraints. *Automatica*, 44(5):1343–1349, 2008.

[6] J. Lieberman and C. Breazeal. TIKL: Development of a wearable vibrotactile feedback suit for improved human motor learning. *IEEE Trans. Robot.*, 23(5):919–926, 2007.

[7] R.W. Lindeman, Y. Yanagida, H. Noma, and K. Hosaka. Wearable vibrotactile systems for virtual contact and information display. In *Virtual Reality*, volume 9, pages 203–213. 2006.

[8] S. Scheggi, F. Chinello, and D. Prattichizzo. Vibrotactile haptic feedback for human-robot interaction in leader-follower tasks. In *ACM PETRA Workshop on Robotics in Assistive Environments*, pages 1–4, 2012.

[9] R. Gockley, J. Forlizzi, and R.G. Simmons. Natural person-following behavior for social robots. In *Proc. ACM/IEEE Int. Conf. on Human-Robot Interaction*, pages 17–24, 2007.

[10] M. Loper, O.C. Jenkins, N. Koenig, S. Chernova, and C. Jones. Mobile human-robot teaming with environmental tolerance. In *Proc. ACM/IEEE Int. Conf. Human-Robot Inter.*, pages 157–164, 2008.

[11] K. Morioka, Joo-Ho Lee, and H. Hashimoto. Human-following mobile robot in a distributed intelligent sensor network. *IEEE Trans. Ind. Electron*, 51(1):229–237, 2004.

[12] J. Saez-Pons, L. Alboul, and J. Penders. Experiments in cooperative human multi-robot navigation. In *Proc. IEEE Int. Conf. Robot. Automat*, pages 1–4, 2011.

[13] L. Nomdedeu, J. Sales, E. Cervera, J. Alemany, R. Sebastia, J. Penders, and V. Gazi. An experiment on squad navigation of human and robots. In *Proc. IEEE Int. Conf. on Control, Automation, Robotics and Vision*, pages 1212–1218, 2008.

[14] F. Sergi, D. Accoto, D. Campolo, and E. Guglielmelli. Forearm orientation guidance with a vibrotactile feedback bracelet: On the directionality of tactile motor communication. In *Proc. IEEE RAS EMBS Int. Conf. on Biomedical Robotics and Biomechatronics*, pages 433–438, 2008.

[15] M. Matscheko, A. Ferscha, A. Riener, and M. Lehner. Tactor placement in wrist worn wearables. In *Proc. Int. Symp. Wearable Computers*, 2010.

[16] W. Guo, W. Ni, I-M. Chen, Z. Qiang Ding, and S. H. Yeo. Intuitive vibro-tactile feedback for human body movement guidance. In *Proc. IEEE Int. Conf. Robotics and Biomimetics*, pages 135–140, 2009.

[17] A.A. Stanley and K.J. Kuchenbecker. Evaluation of Tactile Feedback Methods for Wrist Rotation Guidance. *IEEE Trans. Haptics*, 5(3):240–251, 2012.

[18] J. B. F. Van Erp, H. A. H. C. Van Veen, Chris C. Jansen, and T. Dobbins. Waypoint navigation with a vibrotactile waist belt. *ACM Trans. Appl. Percept.*, 2(2):106–117, 2005.

[19] K. Tsukada and M. Yasumura. ActiveBelt: Belt-Type Wearable Tactile Display for Directional Navigation. In *UbiComp: Ubiquitous Computing*, volume 3205 of *Lecture Notes in Computer Science*, pages 384–399. 2004.

[20] L. Consolini, F. Morbidi, D. Prattichizzo, and M. Tosques. On a class of hierarchical formations of unicycles and their internal dynamics. *IEEE Trans. Automat. Contr.*, 57(4):845–859, 2012.

[21] D.M. Stipanović, P.F. Hokayem, M.W. Spong, and D.D. Šiljak. Cooperative Avoidance Control for Multiagent Systems. *ASME J. Dyn. Syst. Meas. Contr.*, 129(5):699–707, 2007.

[22] Q. Zhang and R. Pless. Extrinsic calibration of a camera

and laser range finder (improves camera calibration). In *Proc. IEEE/RSJ Int. Conf. Intel. Robots Syst.*, pages 2301–2306, 2004.
[23] F. Gemperle, T. Hirsch, A. Goode, J. Pearce, D. Siewiorek, and A. Smailigic. Wearable vibro-tactile display, 2003. Carnegie Mellon University.
[24] L.A. Jones and S.J. Lederman. *Human hand function*. Oxford University Press, 2006.
[25] I. Karuei, K. E. MacLean, Z. Foley-Fisher, R. MacKenzie, S. Koch, and M. El-Zohairy. Detecting vibrations across the body in mobile contexts. In *Proc. Int. Conf. on Human Factors in Computing Systems*, pages 3267–3276, 2011.
[26] L. J. Post, I. C. Zompa, and C. E. Chapman. Perception of vibrotactile stimuli during motor activity in human subjects. *Exp. Brain Res.*, 100:107–120, 1994.
[27] S. Weinstein. Intensive and extensive aspects of tactile sensitivity as a function of body part, sex, and laterality. In *The skin senses*, pages 195–218. Erlbaum, 1968.
[28] R. S. Johansson. Tactile sensibility in the human hand: receptive field characteristics of mechanoreceptive units in the glabrous skin. *The Journal of Physiology*, 281(1), 1978.
[29] A. Riener. Sensor-actuator supported implicit interaction in driver assistance systems. In S. Hölldobler et al., editor, *Ausgezeichnete Informatikdissertationen 2009*, volume 10, pages 221–230. 2010.
[30] S. Schätzle, T. Ende, T. Wüsthoff, and C. Preusche. Vibrotac: An ergonomic and versatile usable vibrotactile feedback device. In *Proc. IEEE Int. Symp. on Robot and Human Interactive Communication*, pages 670–675, 2010.
[31] I.M. Vogels, A.M. Kappers, and J.J. Koenderink. Haptic aftereffect of curved surfaces. *Perception*, 25(1):109–119, 1996.
[32] M. J. Griffin. *Handbook of human vibration*. Elsevier, 1996.
[33] R.W. Cholewiak and A.A. Collins. Sensory and Physiological Bases of Touch. In M.A. Heller and W. Schiff, editors, *The Psychology of Touch*, chapter 2, pages 23–60. Erlbaum, 1991.
[34] T. N. Cornsweet. The staircase-method in psychophysics. *Am. J. Psychol.*, 75(3):485–491, 1962.
[35] R. G. Miller. *Beyond ANOVA: basics of applied statistics*. Chapman & Hall, 1997.
[36] R. B. Rusu and S. Cousins. 3D is here: Point Cloud Library (PCL). In *Proc. IEEE Int. Conf. Robot. Automat*, pages 1–4, 2011.

Stefano Scheggi (S'09 - M'12) received the M.S. degree and Ph.D. degree in Information Engineering from the University of Siena, Italy, in 2007 and 2012, respectively. He was a Visiting Scholar at the Department of Computer Science, George Mason University, Fairfax, USA, for six months in 2011, under the supervision of Prof. Jana Košecká. From September 2012, he holds a postdoctoral position at the University of Siena, Italy. His research interests include computer vision, visual servoing, mobile robotics, haptics and augmented/virtual reality.

Fabio Morbidi (S'07 - A'09 - M'12) received the M.S. degree in Information Engineering and Ph.D. degree in Robotics and Automation from the University of Siena, Italy, in 2005 and 2009, respectively. He was a Visiting Scholar at the Center for Control, Dynamical Systems and Computation (CCDC), University of California, Santa Barbara, USA, for six months in 2007-2008. He held postdoctoral positions at the University of Siena, Northwestern University, USA, and University of Texas at Arlington, USA. Since November 2012, he has been with the Networked Controlled System (NeCS) team, Inria Grenoble Rhône-Alpes, France. His research interests include multi-agent systems, distributed control, robot vision and road traffic estimation.

Domenico Prattichizzo (S'93 - M'95) received the M.S. degree in Electronics Engineering and the Ph.D. degree in Robotics and Automation from the University of Pisa in 1991 and 1995, respectively. Since 2002 Associate Professor of Robotics at the University of Siena. Since 2009 Scientific Consultant at Istituto Italiano di Tecnoloogia, Italy. In 1994, Visiting Scientist at the MIT AI Lab. Guest Co-Editor of Special Issue "Robotics and Neuroscience" of the Brain Research Bulletin (2008). Co-author of the "Grasping" chapter of "Handbook of Robotics" Springer, 2008, awarded with two PROSE Awards presented by the American Association of Publishers. Since 2014, Associate Editor of Frontiers of Biomedical Robotics. From 2007 to 2013 Associate Editor in Chief of the IEEE Trans. on Haptics. From 2003 to 2007, Associate Editor of the IEEE Trans on Robotics and IEEE Trans. on Control Systems Technologies. From 2013 Chair of the IEEE RAS Early Carreer Awards Evaluation Panel. Vice-chair for Special Issues of the IEEE Technical Committee on Haptics (2006-2010). Chair of the Italian Chapter of the IEEE RAS (2006-2010), awarded with the IEEE 2009 Chapter of the Year Award. Co-editor of two books by STAR, Springer Tracks in Advanced Robotics, Springer (2003, 2005). Research interests are in haptics, grasping, visual servoing, mobile robotics and geometric control. Author of more than 200 papers in those fields. Leader of a research unit in four EU projects: ROBOCAST, THE, ACTIVE, DALI. Coordinator of the EU ECHORD-EXPERIMENT HANDS.DVI. From March 2013 Coordinator of the IP collaborative project "WEARable HAPtics for Humans and Robots" (WEARHAP).